

L-BAND INSAR DECORRELATION ANALYSIS IN VOLCANIC TERRAINS USING AIRBORNE LIDAR DATA AND *IN SITU* MEASUREMENTS: THE CASE OF THE PITON DE LA FOURNAISE VOLCANO, FRANCE

Mélanie Sedze^{1,2}, Essam Heggy³, Frédéric Bretar⁴, Daniel Berveiller⁵ and Stéphane Jacquemoud¹

(1) Institut de Physique du Globe de Paris, Paris, France, (2) Institut National de l'Information Géographique et Forestière, Saint-Mandé, France, (3) Jet Propulsion Laboratory, Pasadena, USA, (4) CETE Normandie-Centre, Grand Quevilly, France, (5) Laboratoire Ecologie, Systématique et Evolution, Orsay, France

ABSTRACT

We combine ALOS-PALSAR coherence images with airborne LiDAR data, both acquired over the Piton de la Fournaise volcano (Reunion Island, France), to study the main errors affecting repeat-pass InSAR measurements and understand their causes. The high resolution DTM generated using LiDAR data is used to subtract out the topographic contribution from the interferogram and to improve the radar coherence maps. The relationship between LiDAR intensity and radar coherence is then analyzed over several typical volcanic surfaces: it helps to evaluate the coherence loss terms. Additionally, the geometric and physical properties of these surfaces have been measured *in situ*. Coherence deteriorates over pyroclastic deposits and rough lava flows due to volume and surface scattering. In the presence of vegetation, it is directly related to plant density: the higher the Leaf Area Index (LAI), the lower the coherence. The accuracy of InSAR measurements strongly decreases for LAI higher than 7.

Index Terms— Radar coherence, LiDAR, Piton de la Fournaise volcano

1. INTRODUCTION

Understanding the forces that shape the earth's crust requires accurate topographic maps, as well as an adequate spatial and temporal coverage. Over the past years, synthetic aperture radar interferometry (InSAR) proved to be a very effective tool to quantitatively describe the earth's surface and its physical properties. It is now routinely used to map terrain topography and monitor high-resolution and large-scale ground displacements, in particular over active volcanoes like the Piton de la Fournaise (Reunion Island, France) [3], [4], with a vertical accuracy equal to a fraction of the wavelength (a few centimeters). However, our ability to measure such volcanic deformations using SAR interferometry depends on our ability to maintain phase coherence over the surveyed surfaces and over appropriate slots. In areas subject to multiple eruptive periods, the availability of an accurate and updated digital terrain model

(DTM) remains challenging. All these restrictions lead to spatial and temporal ambiguities associated with InSAR monitoring of volcanic activity. During the past decade, laser altimetry using a LiDAR (Light Detection and Ranging) has been increasingly used to collect high-resolution topographic data and generate DTM with a vertical accuracy lower than 20 cm [1]. The properties of the laser beam to penetrate through vegetation allows this technique to obtain information both on the terrain topography and the structure of vegetation cover, and enables a good estimate of biomass [10]. LiDAR has been used in a wide range of applications including volcanology [8]. The intensity, amount of energy reflected by the target, has been recently used to identify and map different volcanic products such as lava and pyroclastic flows, as well as fallout deposits [2], [9]. To date radar/LiDAR fusion has been very little investigated in the literature. The main studies aim at better assessing plant canopy height [11] and biomass [14], or the ground's surface under foliage to improve InSAR-derived elevation estimates [12].

In this paper, we combine airborne LiDAR data with spaceborne InSAR coherence images from ALOS/PALSAR (Advanced Land Observing Satellite / Phased Array type L-band Synthetic Aperture Radar) acquired over the Piton de la Fournaise in 2008 and 2009. We investigate how phase coherence varies with the nature of volcanic terrains and vegetation density in a typical volcanic environment. Our study provides insights for future SAR missions such as the U.S. DESDynI (Deformation, Ecosystem Structure and Dynamics of Ice) mission, which will combine spaceborne radar and LiDAR measurements to address issues in solid earth sciences.

2. DATA COLLECTION

2.1. LiDAR datasets

Two airborne LiDAR survey missions were conducted in October 2008 and 2009 over the Piton de La Fournaise volcano by the Institut National de l'Information Géographique et Forestière (IGN) using an Optech ALTM 3100 system operating in the near infrared domain (1.064

μm). The data were acquired at an altitude of approximately 1,400 m above ground level with a scanning angle ranging from 0° to 10°.

2.1.1. DTM generation

A filtering routine is first applied to the raw LiDAR data to separate ground points from non-ground points, which correspond to the top of vegetation canopies in that case. Once the point cloud is classified, an accurate DTM of the volcano (5 m spatial resolution) is built by interpolating the ground points using the Terrascan® software.

2.1.2. Normalized LiDAR intensity

LiDAR intensity is the amplitude signal of the laser return measured by the system. It is expressed as a positive digital number (I). A radiometric correction model is applied to remove some influential factors (sensor-target range, slope) and obtain reliable intensity values, which allow a textural and spectral characterization of the volcanic terrains. This model is based on the radar equation (Eq. 1) [5]. We neglect the atmospheric attenuation because the weather was clear during the flights.

$$I_{corrected} = I \times \left(\frac{R}{R_s}\right)^2 \times \frac{1}{\cos(\alpha)} \quad (1)$$

With $I_{corrected}$ the corrected intensity, R the recorded range, R_s the standard altitude, and α the incidence angle.

2.2. PALSAR images

Several ALOS/PALSAR images have been processed in this study. PALSAR is a L-band radar at the center frequency of 1.27 GHz (wavelength of 23.6 cm). The Reunion Island site has been selected for the nighttime ascending acquisition plans. The images were acquired at off-nadir angle (34.3°), in single (HH) or dual (HH and HV) polarimetric modes, from March 2008 to September 2010. To study the radar-LiDAR complementarity, we selected the best image pair on several criteria: the slot between two radar images must overlap the LiDAR survey period; the baseline separation must be lower than 1 km; and the temporal baseline must be short to limit geometric and temporal decorrelation. Since a limited number of images were available in 2009, we chose the two acquired on September 6, 2008 and October 22, 2008 in HH polarimetric mode. The spatial perpendicular baseline has been estimated at 357 m (critical perpendicular baseline = 6635 m) and the slot equals 46 days. The single look complex images were processed using the SARscape module from ENVI.

3. COHERENCE ESTIMATE

In SAR interferometry, the coherence γ is defined as the magnitude of the cross-correlation coefficient between two co-registered complex images. It ranges from 0 (no correlation) to 1 (perfect correlation). γ is estimated by

ensemble averaging the complex signals z_1 and z_2 within a window:

$$\gamma = \frac{|\sum_{i=1}^L z_{1i} z_{2i}^*|}{\sqrt{\sum_{i=1}^L |z_{1i}|^2 \sum_{i=1}^L |z_{2i}|^2}} \quad (2)$$

Where $*$ stands for the complex conjugate and $L = n_{az} \times n_r$ is the total number of pixels averaged in azimuth and range. The correlation coefficient was generated for the selected image pair with 1 look in the range direction and 8 looks in the azimuth direction. It yields a square pixel size of ~ 25 m. Before estimating the coherence, a slope-adaptive spectral filtering is applied to the interferogram to compensate for imaging geometry. The LiDAR-derived DTM is used to remove the topographic effects and obtain an earth-flattened phase factor. Here, the thermal noise is ignored because of the very high SNR in ALOS data. The only significant factors causing decorrelation in the interferogram are consequently the spatial $\gamma_{spatial}$ and temporal $\gamma_{temporal}$ decorrelation factors [16]:

$$\gamma = \gamma_{spatial} \cdot \gamma_{temporal} \quad (3)$$

Indeed, coherence is directly related to surface/volume scattering and temporal stability of surface microwave scattering properties. Loss of coherence can be caused by unstable scatterers (wind effects on foliage, human activity), land cover change (vegetation growth or senescence), and variations in dielectric properties (surface freezing/thawing or wetting/drying). High coherence is generally expected where surface conditions are stable, like urban areas, and low coherence where they may change rapidly, like vegetated areas.

4. ANALYSIS OF COHERENCE VARIATION

The study area encompasses various types of volcanic terrains and vegetation canopies. This environment offers a unique opportunity to analyze and better understand the coherence loss as a function of surface features. To analyze the correlation between interferometric coherence and LiDAR intensity, pixel values of coregistered images are extracted over large homogeneous test regions characterized by high and low coherence. The LiDAR-derived radiometric information allows us to segment the image on the basis of the optical properties of the targets in the near-infrared. Indeed in this wavelength domain, it is quite easy to distinguish between vegetation and bare soils or lava flows.

4.1. Coherence vs volcanic terrain type

We analyzed the coherence over four types of volcanic terrains: pahoehoe and a'a lava flows, slabby pahoehoe flows, and pyroclastic deposits (lapillis). Figure 1 displays LiDAR-InSAR histogram patterns that are typical of each surface: (1) pyroclastic deposits and a'a lava flows are characterized by low coherence (0.48 ± 0.07 / 0.62 ± 0.06) and intensity (0.11 ± 0.007 / 0.20 ± 0.02) values, with high

coherence standard deviations; (2) pahoehoe and slabby lava flows are characterized by high coherence and intensity values, with low standard deviations.

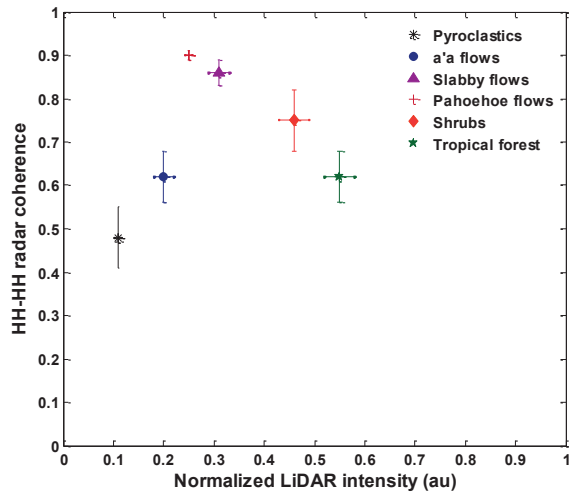


Figure 1: Correlation between HH-HH radar coherence and normalized LiDAR intensity for different types of volcanic terrains.

The physical properties of a few typical surfaces of the Piton de la Fournaise have been studied in October 2011 in the frame of a geological survey. From digital photographs, we first computed $\sim 25\text{m}^2$ DTM at 1 mm spatial resolution using a software for automatic image matching. Several 4 m long 1D-profiles have been extracted from these surfaces in order to calculate three roughness parameters: the standard deviation of height σ , the correlation length L_c , and a new parameter Z_s introduced by [17]. It is defined as $Z_s = \sigma^2/L_c$ and takes into account both the vertical and horizontal roughness components. Table 1 displays the mean values of σ , L_c , and Z_s . These parameters are specific to a terrain type: the rougher the surface, the lower the correlation length, and the higher the standard deviation of height, as well as Z_s . These textural characteristics confirm what we know intuitively, namely that the a'a lava flows are rougher than the pahoehoe and slabby lava flows, whereas the pyroclastic deposits are very flat.

Surface type	σ (cm)	L_c (cm)	Z_s (cm)
a'a lava flow	7.5 ± 1.1	20.1 ± 9.2	3.7 ± 1.5
Pahoehoe lava flow	4.6 ± 0.4	30.6 ± 1.1	0.8 ± 0.2
Slabby lava flow	3.7 ± 1.4	26.4 ± 5.3	0.7 ± 0.4
Pyroclastic deposit	0.7 ± 0.2	43.3 ± 8.2	0.01 ± 0.01

Table 1: Surface roughness parameters of several volcanic terrains.

These quantitative results help us to better understand how electromagnetic waves interact with such surfaces: very rough and porous surfaces (a'a lava flows) produce multiple scattering so that the sum of backscatter signals in a radar cell is less coherent than for a smoother surface (pahoehoe lava flows). As far as the LiDAR reflectivity is concerned, it doesn't seem to be affected by the geometrical features of

the surface. Moreover, the coherence loss observed over the smooth pyroclastic covers is not due to surface scattering but caused by volumetric effects. Here, the radar signals are decorrelated owing to radar wave penetration into the pyroclastic layers. Deep penetration of microwaves is frequency and site dependent. Typically, the relative permittivity (dielectric constant) and the conductivity of the deposits, which are directly related to lithology (i.e., clay content), play a key role since they influence the radar wave interaction with the geological medium. For instance, volcanic deposits are highly resistive and compositionally homogeneous, which causes significant radar wave absorption and facilitates deep penetration of radar energy [6]. To quantitatively evaluate the importance of the volume scattering, we will assess the penetration depth δ_p over volcanic deposit layers in the Plaine des Sables [7]:

$$\delta_p \approx \frac{\lambda \sqrt{\varepsilon'}}{2\pi \varepsilon''} \quad (4)$$

Where λ is the radar wavelength, ε' and ε'' are the real part and the imaginary part of the complex dielectric constant of the medium respectively.

4.2. Coherence vs vegetation density

The radar signal is also subject to volume scattering over vegetation due to the architecture, density and height of plant canopies. L-band radar signals, which penetrate relatively thin vegetation layers deeper than shorter ones (e.g., 6-cm C-band) tend to mitigate this effect and display higher coherence values over canopy [15]. The LiDAR-InSAR relationship was also analyzed over vegetated sites (Fig. 1). Coherence decreases in regions with dense vegetation, whereas LiDAR intensity increases. Moreover, we observed a higher dispersion of coherence and intensity values depending on the type and density of plants. For these covers, the laser pulses are reflected before hitting the bare ground generating a mixed signal from ground and vegetation layers.

During the 2011 geological survey, we performed *in situ* measurements of the LAI (Leaf Area Index) using the LAI-2000 Plant Canopy Analyzer over sparse vegetation (shrubs in the Plaine des Sables) and tropical forest (ferns and trees in the Grand Brûlé). The LAI reflects vegetation density. Moreover, we processed several SPOT 5 images calibrated into reflectance (<http://kalideos.cnes.fr/>) to produce NDVI (Normalized Difference Vegetation Index) maps at 10 m spatial resolution. Both field and satellite data helped us to establish the LAI-NDVI relationship [13] in order to generate LAI maps from SPOT images. Very low temporal variations have been noticed in tropical plants between 2008 and 2011, so we used the LAI maps generated from a SPOT image acquired on May 2011. Coherence and LAI data were extracted over homogeneous areas characterized by different vegetation density. Figure 2 shows a good negative correlation between the two values: coherence decreases

when LAI increases. For LAI values higher than 7, measuring ground deformations with a radar might be very difficult or even impossible. The wind effect on the radar coherence should take into account for a better analysis.

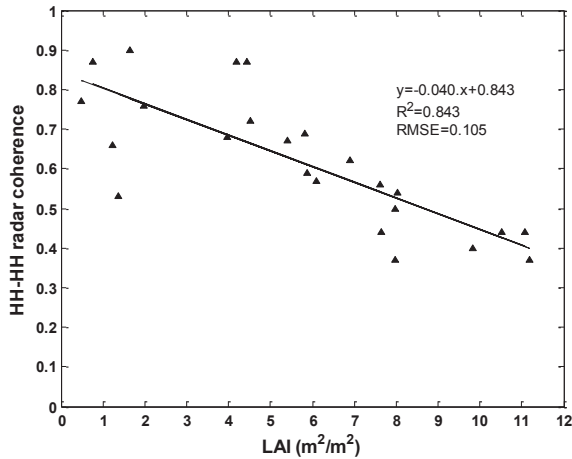


Figure 2: Correlation between HH-HH radar coherence and Leaf Area Index (LAI) for different vegetated surfaces.

5. CONCLUSION

This study aims at better interpreting the spatial and temporal behaviors of the L-band backscattering coefficient over different types of volcanic terrains and vegetated covers. To do this, normalized LiDAR intensities were statistically correlated to L-band HH-HH coherences on various areas of the volcano covered by lava flows, pyroclasts, and vegetation. Surface roughness parameters and LAI maps have been also used to describe the geometrical properties of the ground and the vegetation density, respectively. Such studies allow us to discriminate between scattering and volumetric effects: we observe high coherence loss over rougher a lava flow in the Enclos Fouqué due to multiple scattering of the radar waves and over pyroclastic deposits in the Plaine des Sables caused by radar wave penetration into the medium. Over vegetated areas, the radar coherence is directly related to the LAI: the higher the LAI, the lower the coherence. This correlation that is showed for the first time in this study will be used to develop empirical models to correct for the L-band phase distortion. It should enhance the monitoring of pre-eruptive surface deformations.

ACKNOWLEDGMENTS

This study was funded by the French Space Agency (CNES) in the frame of the program “Terre Océan Surfaces Continentales Atmosphère”.

REFERENCES

- [1] Baltasvias, E.P., “Airborne laser scanning: existing systems and firms and other Resources”, *ISPRS Journal of Photogrammetry & Remote Sensing*, 54, pp. 164-198, 1999.
- [2] Fornaciai A., Bisson M., Landi P., Mazzarini F. and Pareschi M.T., “A LiDAR survey of Stromboli volcano (Italy): digital elevation model-based geomorphology and intensity analysis”, *International Journal of Remote Sensing*, 31, pp. 3177-3194, 2010.
- [3] Froger J.L., Fukushima Y., Briole P., Staudacher T., Souriot T. and Villeneuve N., “The deformation field of the August 2003 eruption at Piton de la Fournaise, Reunion Island, mapped by ASAR interferometry”, *Geophysical Research Letters*, 31:L14601, 2004.
- [4] Fukushima, Y., Cayol V. and Durand P., “Finding realistic dike models from interferometric synthetic aperture radar data: The February 2000 eruption at Piton de la Fournaise”, *Journal of Geophysical Research*, 110, B03206, doi:10.1029/2004JB003268, 2005.
- [5] Höfle B. and Pfeifer N., “Correction of laser scanning intensity data: data and model-driven approaches”, *ISPRS Journal of Photogrammetry and Remote Sensing*, 62, pp. 415-433, 2007.
- [6] Kruse S., Mora R., Ramirez C. and Alvarado G., “Ground penetrating radar imaging of tephra stratigraphy on Poás and Irazú volcanoes, Costa Rica”, *Revista Geológica de América Central*, 43, pp. 119-136, 2010.
- [7] Massonnet D. and Souyris J.C., “Imaging with synthetic aperture radar”, EPFL Press, 2008.
- [8] Mazzarini F., Pareschi M.T., Favalli M., Isola I., Tarquini S. and Boschi E., “Morphology of basaltic lava channels during the Mt. Etna September 2004 eruption from airborne laser altimeter data”, *Geophysical Research Letters*, 32:L04305, 2005.
- [9] Mazzarini F., Pareschi M. T., Favalli M., Isola I., Tarquini S. and Boschi E., “Lava flow identification and aging by means of lidar intensity: Mount Etna case”, *Journal of Geophysical Research*, 112:B02201, 2007.
- [10] Nillson M., “Estimation of tree heights and stand volume using airborne Lidar system”, *Remote Sensing Environment*, 56, pp. 1-7, 1996.
- [11] Sexton J.O., Bax T., Siqueira P., Swenson J.J. and Hensley S., “A comparison of lidar, radar, and field measurements of canopy height in pine and hardwood forests of southeastern North America”, *Forest Ecology and Management*, 257:1136-1147, 2009.
- [12] Slatton K.C., Crawford M.M. and Evans B.L., “Fusing interferometric Radar and Laser altimeter data to estimate surface topography and vegetation heights”, *IEEE Transactions on Geoscience and Remote Sensing*, 39, pp. 2470-2482, 2001.
- [13] Steltzer H. and Welker J.M., “Modeling the effect of photosynthetic vegetation properties on the NDVI-LAI relationship”, *Ecology*, 87, pp. 2765-2772, 2006.
- [14] Sun G., Jon Ranson K., Guo Z., Zhang Z., Montesano P. and Kimes D., “Forest biomass mapping from lidar and radar synergies”, *Remote Sensing of Environment*, 115, pp. 2906-2916, 2011.
- [15] Wei M. and Sandwell D.T., “Decorrelation of L-band and C-band interferometry over vegetated areas in California”, *IEEE Transactions on Geoscience and Remote Sensing*, 48, pp. 2942-2952, 2010.
- [16] Zebker H.A. and Villasenor J., “Decorrelation in interferometric radar echoes”, *IEEE Transactions on Geoscience and Remote Sensing*, 30(5), pp. 950-959, 1992.
- [17] Zbri M. and Dechambre M., “A new empirical model to retrieve soil moisture and roughness from C-band radar data”, *Remote Sensing of Environment*, 84, pp. 42-52, 2002.